J Appl Electrochem (2007) 37:1077–1084
DOI 10.1007/s10800-007-9358-5

ORIGINAL PAPER

Catalysed titanium mesh electrodes for ethylene glycol fuel cells

Raghuram Chetty · Keith Scott

Received: 15 November 2006 / Revised: 25 June 2007 / Accepted: 25 June 2007 / Published online: 20 July 2007

Abstract Electrodes comprising thermally deposited Pt, PtRu and PtRuW on titanium mesh were evaluated for the oxidation of ethylene glycol in acidic electrolyte. The electrodes were characterised using cyclic voltammetry, scanning electron microscopy and X-ray diffraction and the effect of reactant concentration and temperature were examined. Single fuel cell tests employing the titanium mesh anode with the PtRuW catalyst showed better performance than that of the PtRu catalyst. A peak power density of 15 mW cm^{-2} was obtained at a temperature of 90 °C with 1.0 M ethylene glycol solution. The performance of the catalysed PtRu mesh electrode was comparable to that of a commercial, alcohol oxidation, PtRu carbon supported catalyst.

Keywords Titanium mesh · Ethylene glycol · Oxidation · Electrocatalyst · Platinum ruthenium · Tungsten · Fuel cells

1 Introduction

The electrochemical oxidation of ethylene glycol on noble metal catalysts has received considerable attention in recent years due to its potential application in direct alcohol fuel cells [1–10]. Methanol has been considered one of the more promising fuels for fuel cells as it can be oxidised more efficiently than other alcohols. However, methanol is toxic and methanol crossover results in a decrease in efficiency [11, 12]. Ethylene glycol is more efficient and safer than methanol and has a theoretical volumetric energy capacity (Ah ml^{-1}) 17% higher than that of methanol [1]. Moreover, ethylene glycol is well known in automobile and other transport industries and distribution networks already exist. Thus it is a possible alternative fuel for transport and mobile applications [6].

In a fuel cell, the ideal oxidation of ethylene glycol is:

$$C_2H_6O_2 + 2\ H_2O \rightarrow 2\ CO_2 + 10\ H^+ + 10\ e^- \quad (1)$$

However, the mechanism of ethylene glycol electrooxidation is complex and active and selective anode electrocatalysts are required. On platinum, ethylene glycol oxidation occurs via a parallel reaction mechanism with numerous intermediate steps. These steps involve oxidation of functional groups (–OH) without C–C bond rupture, in the one path, and splitting of the C–C bond with formation and oxidation of adsorbed CO in the second path [10]. Previous studies have shown that, in addition to CO_2, ethylene glycol oxidation products include C2 molecules such as glycolaldehyde, glyoxal, glycolic acid, glyoxylic acid and oxalic acid and C1 molecules, such as formaldehyde and formic acid [13–16].

Although platinum is considered to be an active catalyst for oxidation of alcohols in acid solutions [14–18], the formation of poisoning CO species, which adsorb onto the platinum catalyst, block its active sites and limit the oxidation ability. Hence, modification of the Pt catalyst is used to reduce the formation of strongly absorbed species or to remove the CO species by oxidation at lower potentials. A typical modification is the use of binary and ternary Pt alloys with Ru, Sn, Mo, Ni, W [19, 20]. Addition of a second and third metal can result in dissociation of C–H or

R. Chetty (✉) · K. Scott
School of Chemical Engineering & Advanced Materials,
Newcastle University, Newcastle upon Tyne NE1 7RU, UK
e-mail: raghuram.chetty@ncl.ac.uk

K. Scott
e-mail: k.scott@ncl.ac.uk

C–C bonds and complete oxidation to CO_2 by the bi-functional mechanism [10, 18, 21]:

$$Pt + CO \rightarrow Pt{-}CO_{ads} \quad (2)$$

$$M + H_2O \rightarrow M{-}OH_{ads} + H^+ + e^- \quad (M = Ru,\ Sn,\ W,\ Ni,\ etc.) \quad (3)$$

$$Pt{-}CO_{ads} + M{-}OH_{ads} \rightarrow CO_2 + Pt + M + H^+ + e^- \quad (4)$$

Recently, Peled et al. [1] reported an ethylene glycol fuel cell, equipped with a new nano-porous proton-conducting membrane and a PtRu/C anode catalyst, with a power density of 320 mW cm^{-2} at 130 °C. This power performance puts ethylene glycol in direct competition with methanol as a potential fuel. Neto et al. [4] observed that an increase in ruthenium or tin content in carbon supported, binary Pt electrocatalysts lowered the electrode potential for ethylene glycol oxidation. Lima et al. [5] also reported that an increase in the ruthenium content in PtRu electrodes increased their activity for ethylene glycol electrooxidation.

The typical anode structure used in alcohol fuel cells consists of successive layers of a supported or unsupported catalyst, bonded with Nafion ionomer, a Teflon bonded carbon black diffusion layer and a carbon cloth or paper diffusion layer [22]. This structure is far from suitable for transport and release of carbon dioxide gas and can result in considerable mass transport limitations of fuel supply at the anode. As a result a gradual deterioration in electrical performance can occur [22, 23].

This paper presents an investigation of Ti mesh supported Pt–Ru electrodes, with the addition of a third metal, such as W, Pd or Ni, for the oxidation of ethylene glycol. The mesh was used because of its three dimensional open structure, which allowed good access for fuel at the reaction interface and enabled efficient gas release. Titanium was used as the electrode substrate because it is electrochemically stable, electronically conducting and a good support for a diverse range of electrocatalysts [23].

Expanded metal titanium substrates are used to make electrodes in several electrochemical industries. Procedures for deposition of catalysts onto such substrates are well known and include thermal, electrochemical and vapour phase deposition. In the proposed fuel cell application the mini-mesh is thin and light and thus low cost. The cost of Ti is approximately half that of Ni, a material commonly used in batteries and alkaline fuel cells, also as mesh. In addition the mesh is flexible and can be formed into a variety of shapes for a range of different fuel cell applications. The hydrophilic nature of the anode assists alcohol transport throughout the electrode structure.

2 Experimental

2.1 Materials

$H_2PtCl_6 \cdot 6H_2O$, $RuCl_3 \cdot xH_2O$, WCl_6, $NiCl_2 \cdot xH_2O$, were obtained from Alfa Aesar, $PdCl_2$, ethylene glycol, sulphuric acid were obtained from Aldrich. Titanium mesh (2Ti5-031) was supplied by Dexmet. The geometric characteristics of the mesh is shown in Fig. 1 and were; strand width (SD) = 0.14 mm, thickness = 0.2 mm and opening size = 1.5 mm (LWD)/0.67 mm (SWD).

2.2 Thermal decomposition

Anodes were prepared by thermal decomposition of Pt based catalyst onto the titanium mesh as described previously [23, 24]. In brief, Ti mesh was repeatedly dipped in a catalyst precursor solution and dried at 100 °C for 10 min until the desired catalyst loading was achieved. The precursor solution was an individual or a mixture of 0.2 M metal chloride in isopropanol. The catalyst coated mesh was then heat treated at 430 °C for 1 h. Electrodes prepared in this way were sonicated in de-ionised water, to remove residual catalyst salts, and the mass of catalyst deposited was determined by weighing.

2.3 Physical characterisation

The electrodes were characterised by X-ray diffraction (XRD) using a Philips X'pert PRO diffractometer operated at 40 kV accelerating voltage and 40 mA beam current and using CuK_α radiation. Analysis of the XRD data was carried out using Philips Xpert High Score. Diffraction peaks were attributed to species according to the Joint Committee of Powder Diffraction Standards (JCPDS) cards. The selected 2θ range was from 20° to 90°, scanning at a step of 0.02°. The surface and cross-sectional morphologies of the anode catalyst layers were examined by a Hitachi S2400 scanning electron microscope (SEM) fitted with an Oxford Instruments Isis 200 Ultra Thin Window X-ray detector, interfaced with energy dispersive X-ray analysis (EDX).

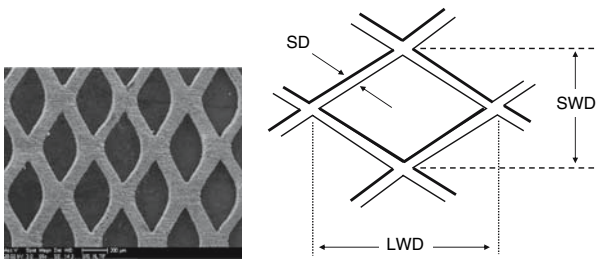

Fig. 1 Titanium mesh (bar = 200 μm) used for thermal decomposition of electrocatalyst

2.4 Electrochemical measurements

Cyclic Voltammetry and chronoamperometry experiments were performed using a PGZ100 Voltalab Radiometer potentiostat, connected to a PC loaded with VoltaMaster software. A conventional three-electrode glass cell, with a reference electrode connected via a Luggin capillary, was used for electrochemical measurements. The temperature of the cell was controlled using a thermostatic water circulator (Grant LTD, Cambridge, UK). The titanium mesh-working electrode was 1 cm^2 in cross sectional area with a 1 mg cm^{-2} catalyst loading. The counter-electrode was platinum mesh and the reference electrode was a mercury sulphate (potential 0.65 V versus RHE). The electrode potentials reported are referenced against the reversible hydrogen electrode (RHE). All experiments were conducted in an N_2 de-aerated electrolyte containing 1 M ethylene glycol in 0.5 M H_2SO_4 unless otherwise stated. Reported current densities are based on the geometric surface area of the anode.

2.5 Membrane electrode assembly

The cathode consisted of a backing layer, a gas diffusion layer and a catalyst layer. The catalyst layer was made from commercial 60 wt.% Pt/C (E-Tek, Lot No. D1260912) catalyst, with a Pt loading of 2 mg cm^{-2}. The backing layer consisted of carbon paper (Toray TGHP-090, E-Tek) onto which a gas diffusion layer (GDL) was applied. The gas diffusion layer consisted of an ultrasonically mixed carbon black (Ketjen black 300), acetone and 10% PTFE suspension. The catalyst layer was then applied to the substrate by spraying an ultrasonically mixed ink of electrocatalyst, Nafion solution (Aldrich) and acetone. The catalysed titanium mesh anode used 2 mg cm^{-2} catalyst loading.

For comparison of performance with mesh anodes, conventional carbon supported anodes were prepared with 2 mg cm^{-2} metal loading of 60 wt.% PtRu/C (E-Tek, Lot No. B0660604) catalyst. The geometric surface areas of the anode and cathode were 2.25 cm^2 and the catalyst loadings of anode and cathode were 2 mg cm^{-2}. Membrane electrode assemblies (MEA) were prepared by hot pressing the anode and cathode either side of a Nafion 117 membrane for 3 min at 130 °C and 100 kg cm^{-2}. The electrodes were coated with 1 mg cm^{-2} of Nafion solution prior to forming a MEA.

Figure 2 shows a comparison of the structure of the conventional anode and the mesh based anode. The conventional anode consisted of a catalyst layer, a microporous layer and a Teflonised carbon cloth or carbon paper backing layer. In contrast the mesh-based anode consisted of one layer, a titanium mesh coated with catalyst, and was thinner than the conventional electrode. Teflon was not used in the mesh anode and hence it was more hydrophilic than the conventional anode.

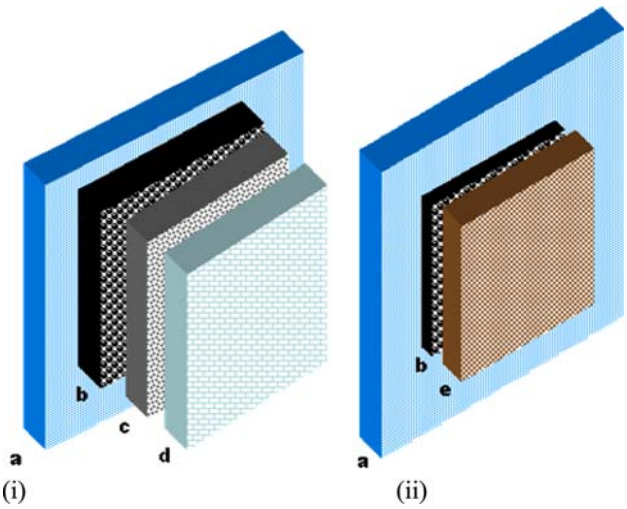

Fig. 2 Schematic representation of (**i**) conventional anode and (**ii**) novel mesh-based anode. (a) Polymer electrolyte membrane, (b) catalyst layer, (c) microporous layer, (d) backing layer and (e) titanium mesh

2.6 Test cells

The cell used to measure performance of MEA consisted of two non-porous graphite blocks with a series of parallel channels machined into the block for the flow of ethylene glycol or oxygen. Prior to data collection, MEA were fully hydrated by feeding Millipore water through the anode compartment at 60 °C for 24 h. The flow rate of 1.0 M ethylene glycol through the anode chamber was 1.0 ml min^{-1} and oxygen flowed through the cathode side of the cell, in stoichiometric excess, at a 1 bar backpressure. A Kenwood PEL-151 electronic load was used to obtain cell polarisation data.

3 Results and discussion

3.1 Physical characterisations

To examine the structural morphology and composition of the catalyst coated mesh electrodes SEM and EDX were employed. Figure 3 shows SEM images of pre-treated titanium mesh and thermally deposited Pt, PtRu and PtRuW anodes. The pre-treated Ti mesh had a rough surface and after catalyst coating the surface layer consisted of a thin (~2 μm) non-crystalline deposit. The deposits had a rough surface, which allowed access of ethylene glycol to the catalyst and produced suitable catalyst activity. The

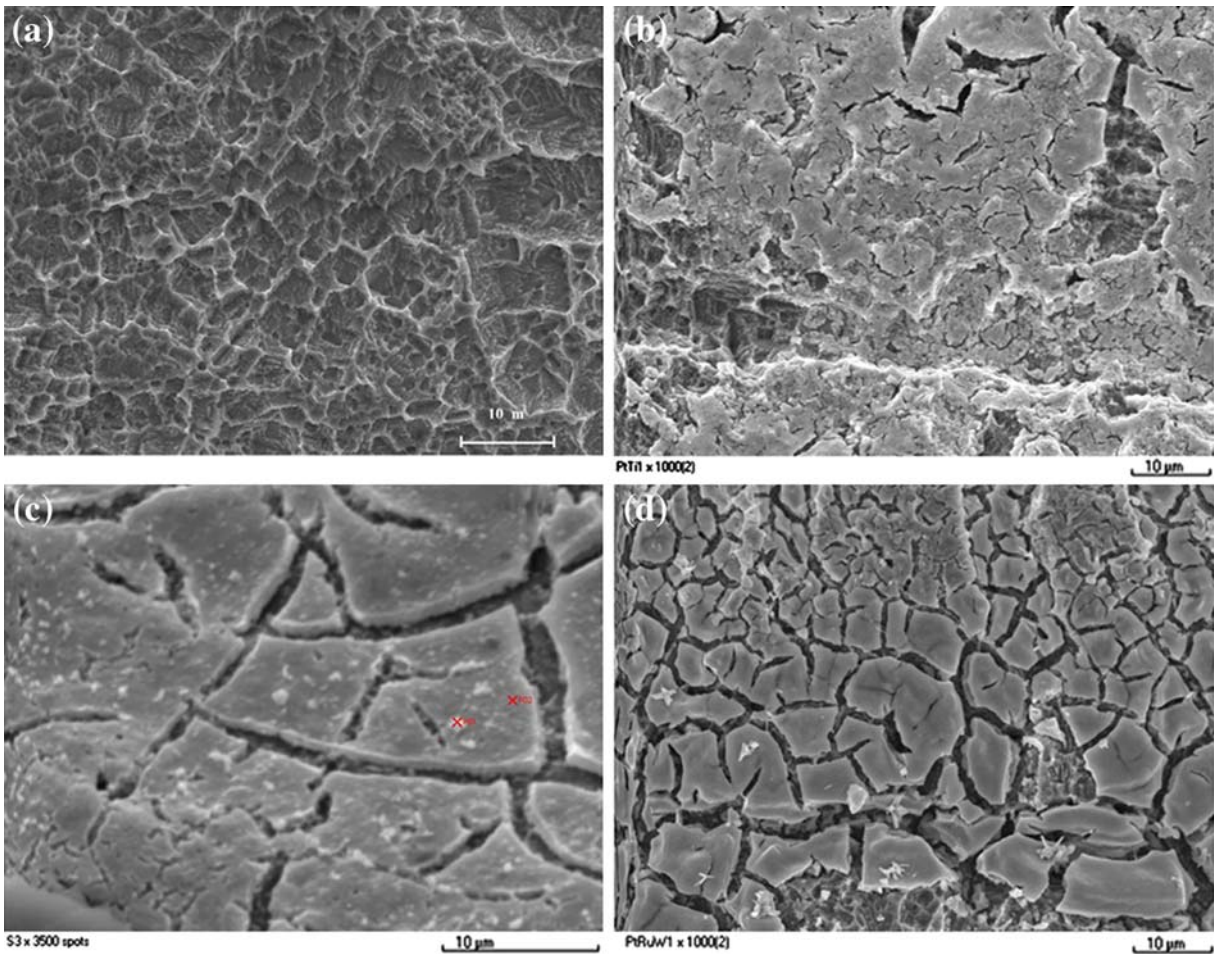

Fig. 3 SEM of (**a**) plain Ti mesh; (**b**) Pt, (**c**) PtRu and (**d**) PtRuW electrocatalyst obtained by thermal decomposition onto titanium mesh (bar = 10 µm)

thermal coatings contained numerous cracks, which were probably created during the decomposition of chlorine compounds and evaporation of water. A typical EDX spectrum is shown in Fig. 4 for the PtRuW mesh electrode. EDX analysis showed that the catalyst coatings were homogeneous and approximate compositions were Pt:Ru, 1:1 and Pt:Ru:W, 1:1:1.

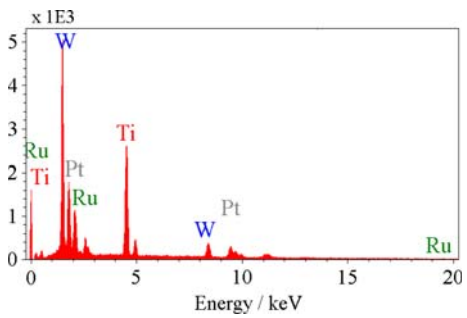

Fig. 4 Energy dispersive X-ray analysis spectrum of the PtRuW/Ti electrode

Figure 5 shows XRD patterns of uncoated titanium mesh and catalyst coated titanium mesh. Typical peaks of the crystalline face centred cubic (fcc) Pt (1 1 1), (2 0 0), (2 2 0) and (3 1 1) planes, and the Ti substrate, are clearly

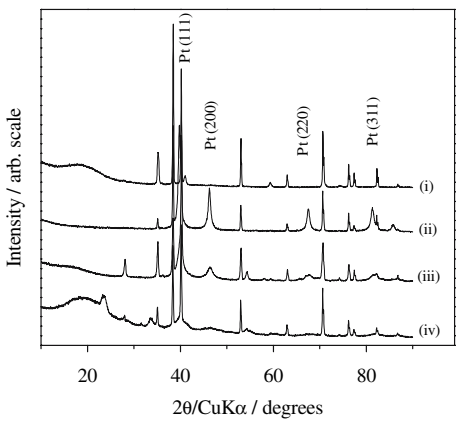

Fig. 5 X-ray diffraction patterns of (i) Ti, (ii) Pt/Ti, (iii) PtRu/Ti and (iv) PtRuW/Ti mesh substrates

visible. Due to its high solubility and smaller atomic size, ruthenium dissolves into the fcc structure of the platinum, displacing the existing Pt atoms, which do not therefore form their own hexagonal close packed lattice. In the case of the PtRuW ternary alloy it is believed that ruthenium dissolves into the orthorhombic crystal structure of Pt_2W to form a solid solution [25]. The mean particle size and lattice parameter obtained from the XRD patterns are summarised in Table 1. The lattice parameter of the (fcc) Pt/Ti was estimated to be 0.3922 nm, while that of the PtRu/Ti and PtRuW/Ti catalysts were 0.3900 and 0.3897 nm respectively, which indicate improved interactions between Pt–Ru and Pt–Ru–W. As evident from the lattice parameters, addition of Ru decreased the lattice parameter of the Pt (fcc) crystal inducing the (2 2 0) reflection peak shift to a higher position. Further investigation is, however, required to correlate the physical differences and activity of the catalysts.

3.2 Cyclic voltammetry

Cyclic voltammograms of thermally decomposed Pt, PtRu and PtRuW, obtained at a scan rate of 20 mV s^{-1} and room temperature, between potentials of 0 and 1.2 V are shown in Fig. 6a. Figure 6b shows the voltammogram of Pt/Ti in 0.5 M H_2SO_4 for comparison and shows typical peaks for hydrogen/oxygen adsorption and desorption on the Pt surface. The peaks were not as sharp and well resolved as for smooth Pt electrode; a possible reason for this is the interaction of Pt with the titanium and titanium oxide species [23]. The shapes of the voltammograms for ethylene glycol oxidation were similar to those reported for carbon-based electrodes [1, 16, 26]. The voltammograms were characterised by a broad peak in the positive sweep, with several maxima, and a single oxidation peak in the negative sweep. Hydrogen adsorption was inhibited by adsorption of ethylene glycol and the oxidation current increased slowly in the double layer region. The oxidation current increased to a maximum around a potential of 900 mV, with a shoulder peak around 700 mV, which may have been due to partial oxidation of ethylene glycol to the different C2 by-products and/or ethylene glycol dissociation to CO_{ads} [1]. The current decreased after reaching the peak at 900 mV; possibly due to oxidation of Pt on the surface leading to a decrease in the number of active sites.

Table 1 Particle size and lattice parameter of the thermally decomposed catalysts

Catalyst	Particle size/nm	Lattice parameter/nm
Pt/Ti	130	0.3922
PtRu/Ti	118	0.3900
PtRuW/Ti	112	0.3897

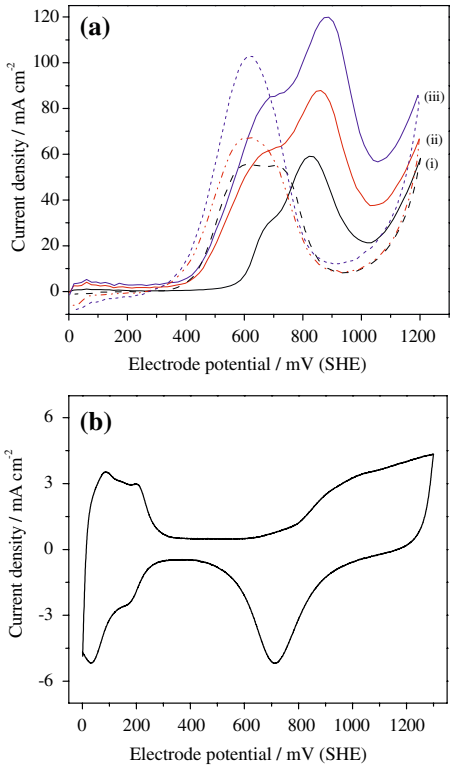

Fig. 6 (**a**) Cyclic voltammograms for oxidation of 1.0 M ethylene glycol in 0.5 M H_2SO_4 at 20 mV s^{-1} scan rate and room temperature. Thermally decomposed (i) Pt//Ti, (ii) PtRu/Ti and (iii) PtRuW/Ti electrodes. Forward scan (solid line) and reverse scan dotted line. (**b**) Cyclic voltammogram of Pt/Ti in 0.5 M H_2SO_4

The single peak in the negative sweep can be attributed to oxidative decomposition of by-products [1].

During cyclic voltammetry the surface structure of anodes containing ruthenium may change, especially at the upper limit of the potential beyond 800 mV. In particular, ruthenium in the electrode may be oxidised and reduced reversibly through a mechanism involving proton exchange with the solution [27]. However, the high potential was applied in this study to examine the overall electrochemical characteristics of the thermally decomposed electrodes. In practical fuel cells the potentials will be well below 800 mV and such changes in the ruthenium oxidation state will be less relevant.

Figure 6a (curves i and ii) demonstrates the enhanced activity of binary and ternary catalysts for ethylene glycol oxidation: greater current densities were obtained, at a given potential, with PtRu and PtRuW compared to Pt. The superior activity obtained with W in the catalyst can be explained by the bi-functional mechanism [25, 28]. In general, the onset potential for alcohol oxidation is attributed to reaction (3). Therefore from the standard potentials, shown in Eqs. (5)–(9), it is possible that W lowered the onset potential for ethylene glycol oxidation. The formation of tungsten oxides during thermal decomposition

cannot be ruled out due to the atmosphere (i.e., air) and high temperature used.

$$PtO + 2H^+ + 2e^- \Leftrightarrow Pt + H_2O \quad (E^o = 0.98V \text{ vs. NHE}) \tag{5}$$

$$Ru_2O_3 + 6H^+ + 6e^- \Leftrightarrow 2Ru + 3H_2O \quad (E^o = 0.74V \text{ vs. NHE}) \tag{6}$$

$$WO_2 + 4H^+ + 4e^- \Leftrightarrow W + 2H_2O \quad (E^o = -0.12V \text{ vs. NHE}) \tag{7}$$

$$W_2O_5 + 2H^+ + 2e^- \Leftrightarrow 2WO_2 + H_2O \quad (E^o = -0.031V \text{ vs. NHE}) \tag{8}$$

$$2WO_3 + 2H^+ + 2e^- \Leftrightarrow W_2O_5 + H_2O \quad (E^o = -0.029V \text{ vs. NHE}) \tag{9}$$

3.3 Ethylene glycol oxidation

Figure 7, shows linear sweep voltammograms (LSV) for ethylene glycol oxidation, obtained at a pseudo-steady state scan rate of 1 mV s^{-1} in the potential range 0–800 mV at 60 °C. The PtRu/Ti electrode showed higher catalytic activity than Pt/Ti. To try to improve the catalytic activity of PtRu, a third metal (M = Ni, Pd and W) was added in the ratio, Pt:Ru:M of 1:1:1. As can be seen in the data, W increased the oxidation current, whereas Pd and Ni had no positive effect. Repeated LSV showed little difference in the oxidation behaviour, which indicated stable performance was achieved using mesh-based anodes. The electrolyte solutions were analysed, with Inductively Coupled Plasma Optical Emission Spectroscopy (ICP-OES, UNICAM 701), before and after polarisation and dissolved metal catalysts were not observed during the short-term polarisation.

Previous research can help to explain the higher catalytic activity of W compared to Pd and Ni in PtRu ternary catalysts. Ishikawa et al. [29] showed that, by using relative density-function calculations, the preferred alloying metals should be those with low-activation energies for H_2O dissociation and for the reaction: $CO_{ads} + OH_{ads} \rightarrow COOH_{ads}$. When $COOH_{ads}$ is formed it rapidly decomposes to CO_{2ads}. Based on energetic predictions, which emphasised water activation, it was predicted that W was one of the more suitable alloying metals for CO electrooxidation.

Pereira et al. [30] reported that, at the potentials experienced by a fuel cell anode, W acted as a redox catalyst, which is present in an oxidised state. The co-catalyst activity was assumed to be due to a rapid change in the oxidation state of W, involving the W(VI)/W(IV) or W(VI)/W(V) redox couples [31]. These redox couples render the W sites active for the dissociative adsorption of water [30].

The different behaviour of the catalysts seen in the LSV (Fig. 7) is demonstrated further in the current-time response curves for the ethylene glycol oxidation, shown in Fig. 8. These curves were measured by polarising the electrode at an oxidation potential of 400 mV for 30 min. The oxidation current initially decreased relatively quickly although the rate of decrease slowed with time for all catalysts. The PtRuW electrode gave the higher oxidation current of 39 mA mg^{-1} cm^{-2}, after 30 min, compared with 29 mA mg^{-1} cm^{-2} and 1 mA mg^{-1} cm^{-2} for PtRu/Ti and Pt/Ti, respectively.

3.3.1 Effect of ethylene glycol concentration

The effect of ethylene glycol concentration on its oxidation at the thermally decomposed PtRuW electrode is shown in

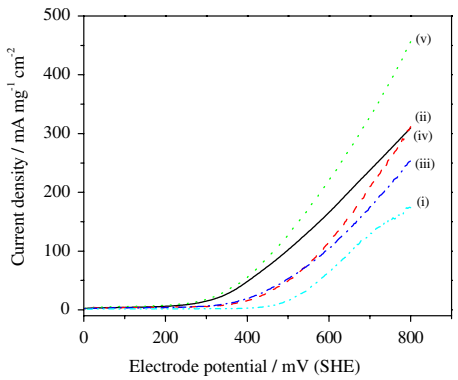

Fig. 7 Linear sweep voltammograms for oxidation of 1.0 M ethylene glycol in 0.5 M H_2SO_4 at 1 mV s^{-1} scan rate at 60 °C on thermally decomposed titanium mesh electrode. (i) Pt, (ii) PtRu (iii) PtRuPd, (iv) PtRuNi and (v) PtRuW

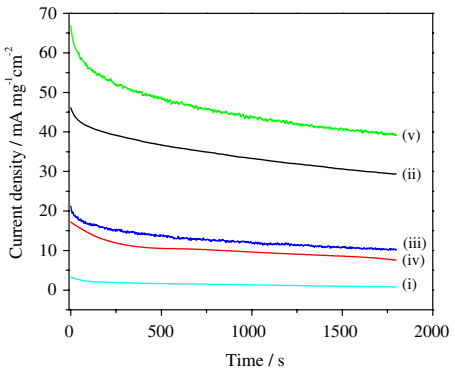

Fig. 8 Chronoamperometric response recorded at 400 mV (SHE) for the oxidation of 1.0 M ethylene glycol in 0.5 M H_2SO_4 at 60 °C on thermally decomposed titanium mesh electrode. (i) Pt, (ii) PtRu (iii) PtRuPd, (iv) PtRuNi and (v) PtRuW

Fig. 9. Current-potential data were obtained in a 0.5 M H_2SO_4 electrolyte at a sweep rate of 1.0 mV s^{-1} and 60 °C with concentrations of 0.1 M, 0.5 M, 1.0 M and 2.0 M ethylene glycol. The lowest concentration (0.1 M) produced the lowest current densities and a limiting current density of less than 200 mA cm^{-2}. The oxidation current increased with an increase in ethylene glycol concentration up to 1.0 M, above which only a small increase in current density was obtained.

3.3.2 Effect of reaction temperature

Figure 10 shows the effect of temperature on the oxidation of ethylene glycol at the thermally decomposed PtRuW electrode. An oxidation current peak was obtained at room temperature (curve i), possibly due to partial oxidation of ethylene glycol to different C2 by-products and/or ethylene glycol dissociation to $CO_{ads,}$ as mentioned earlier. At higher temperatures the oxidation became more facile and higher current densities were observed with increasing temperature from 21 °C to 90 °C. The data agree with the literature on alcohol oxidation; increased oxidation kinetics and lower poisoning by intermediates at higher temperatures.

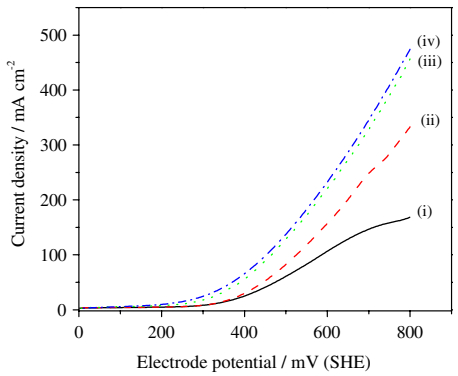

Fig. 9 Effect of ethylene glycol concentration on performance of thermally decomposed PtRuW/Ti electrode. Scan rate 1 mV s^{-1}. (i) 0.1 M, (ii) 0.5 M, (iii) 1.0 M and (iv) 2.0 M

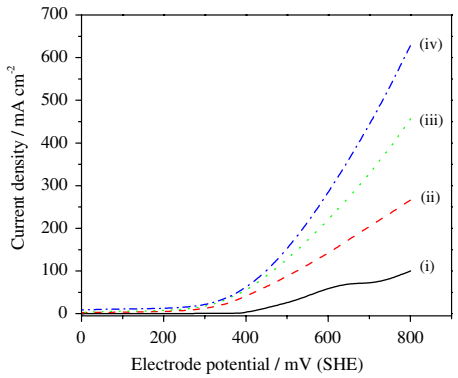

Fig. 10 Effect of temperature on voltammograms for the oxidation of 1.0 M ethylene glycol in 0.5 M H_2SO_4 at 1 mV s^{-1} scan rate on thermally decomposed PtRuW/Ti electrode. (i) 21 ± 1 °C, room temperature (ii) 40 °C (iii) 60 °C and (iv) 90 °C

3.4 Fuel cell polarisation

The activities of the PtRu titanium supported electrodes were evaluated in a direct alcohol fuel cell and compared with that of the carbon-based PtRu/C electrode. Figure 11 compares the cell polarisation curves of commercial PtRu/C and PtRu/Ti mesh anodes at 90 °C and with oxygen at 1.0 bar pressure. The single cell performances of mesh and carbon supported electrodes were comparable under similar operating conditions. Open circuit voltages were approximately 0.47 V for PtRu/Ti and 0.46 V for PtRu/C. Maximum power densities of 10 and 9 mW cm^{-2} were obtained with PtRu/Ti and PtRu/C anodes respectively. The PtRuW/Ti anode gave an open circuit voltage of 0.55 V and a maximum power density of 15 mW cm^{-2}; clearly demonstrating its higher activity for ethylene glycol oxidation. In the low current density region the PtRu anode gave a larger cell voltage loss than the PtRuW anode, indicating higher activation potential losses with the former electrode. Thus it is clear that PtRuW ternary electrocatalysts can provide superior performance to binary alloys for ethylene glycol oxidation.

An attraction of using a mini-mesh-based electrode is the simplicity of electrocatalyst deposition, by dip coating and thermal decomposition. The performance of the mesh-based anode was comparable to, or better than, that of the conventional carbon anode, because of its open structure, which enabled carbon dioxide gas to escape easily from the catalyst layer and which also retained high catalyst utilisation during cell operation. The structure of the mesh gives ready access of ethylene glycol to the catalyst over the majority of its surface.

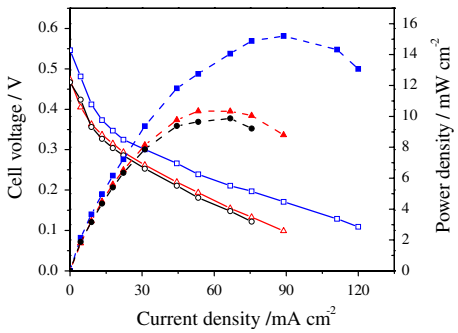

Fig. 11 Fuel cell polarisation data for thermally decomposed PtRuW, PtRu and E-Tek PtRu/C anodes measured at 90 °C in 1 M ethylene glycol and 1 bar oxygen. Anode catalyst loading 2 mg cm^{-2} and cathode catalyst 2 mg cm^{-2} of 60 wt.% Pt/C (E-Tek). Current density (open symbol) and power density (full symbol) for PtRu/C (○, ●), PtRu/Ti (△, ▲) and PtRuW/Ti (□, ■) anodes

An issue that still remains with ethylene glycol oxidation is that at low temperatures, with Pt-based catalysts, complete oxidation to carbon dioxide is not achieved. Several groups are seeking to resolve this problem by trying to develop more active catalysts and by using alternative electrolyte or higher temperatures [1–4]. In this work, although chemical analysis of less oxidised species was not attempted, we would expect C2 and C1 by-products to have formed, even though a slight improvement in activity was achieved with the ternary catalyst. However, what this work has indicated is that improved catalyst activity, achieved with an alternative catalysts substrate, may help reduce by-product formation in combination with other strategies.

4 Conclusions

Platinum-based electrocatalysts deposited on titanium mesh by thermal decomposition of metal salt precursors have been successfully used for oxidation of ethylene glycol in acidic electrolyte. A PtRuW ternary electrocatalyst showed superior performance to PtRu binary and PtRuNi and PtRuPd ternary alloys. The mesh anodes were successfully used in direct ethylene glycol fuel cells and the hydrophilic anode structure produced superior performance to a conventional carbon supported electrode. The mesh-based electrodes have several potential advantages for fuel cell applications, in terms of cost, simplicity, size and shape.

Acknowledgements The authors thank the United Kingdom Engineering and Physical Sciences Research Council for financial support, and Dexmet Corporation, USA for providing titanium mesh.

References

1. Livshits V, Peled E (2006) J Power Sources 161:1187
2. Wang H, Jusys Z, Behm RJ (2006) J Electroanal Chem 595:23
3. Wang H, Zhao Y, Jusys Z, Behm RJ (2006) J Power Sources 155:33
4. Neto AO, Vasconcelos TRR, Da Silva RWRV, Linardi M, Spinace EV (2005) J Appl Electrochem 35:193
5. Lima de RB, Paganin V, Iwasita T, Vielstich W (2003) Electrochim Acta 49:85
6. Peled E, Livshits V, Duvdevani T (2002) J Power Sources 106:245
7. Peled E, Duvdevani T, Aharon A, Melman A (2001) Electrochem Solid-State Lett 4:A38
8. Cherstiouk OV, Savinova ER, Kozhanaova LA, Parmon VN (2000) React Kinet Catal Lett 69:331
9. Ficicioglu F, Kadirgan F (1998) J Electroanal Chem 451:95
10. Wieland B, Lancaster JP, Hoaglund CS, Holota P, Tornquist WJ (1996) Langmuir 12:2594
11. Dillon R, Srinivasan S, Arico AS, Antonucci V (2004) J Power Sources 127:112
12. Arico AS, Srinivasan S, Antonucci V (2001) Fuel Cells 2:133
13. Dailey A, Shin J, Korzeniewski C (1998) Electrochim Acta 44:1147
14. Sun SG, Chen AC, Huang TS, Li JB, Tian ZW (1992) J Electroanal Chem 340:213
15. Orts JM, Vega AF, Feliu JM, Aldaz A, Clavilier J (1990) J Electroanal Chem 290:119
16. Horanyi G, Kazarinov VE, Vassiliev YB, Andreev A (1983) J Electroanal Chem 147:263
17. Iwasita T, Pastor E (1994) Electrochim Acta 39:531
18. Hamnett A (1997) Catalysis Today 38:445
19. Lamy C, Lima A, LeRhun V, Delime F, Coutanceau C, Léger JM (2002) J Power Sources 105:283
20. Zhou WJ, Zhou B, Li WZ, Zhou ZH, Song SQ, Sun GQ, Xin Q, Douvartzides S, Goula M, Tsiakaras P (2004) J Power Sources 126:16
21. Liu H, Song C, Zhang L, Zhang J, Wang H, Wilkinson DP (2006) J Power Sources 155:95
22. Allen RG, Lim C, Yang LX, Scott K, Roy S (2005) J Power Sources 143:142
23. Chetty R, Scott K (2007) J New Mat Electrochem Sys 10:135
24. Chetty R, Scott K (2007) Electrochim Acta 52:4073
25. Tanaka S, Umeda M, Ojima H, Usui Y, Kimura O, Uchida I (2005) J Power Sources 152:34
26. Kadirgan F, Beden B, Lamy C (1982) J Electroanal Chem 136:119
27. Yang LX, Allen RG, Scott K, Christenson PA, Roy S (2005) Electrochim Acta 50:1217
28. Umeda M, Ojima H, Mohamedi M, Uchida I (2004) J Power Sources 136:10
29. Ishikawa Y, Liao MS, Cabrera CR (2002) Surf Sci 513:98
30. Pereira LGS, Santos dos FR, Pereira ME, Paganin VA, Ticianelli EA (2006) Electrochim Acta 51:4061
31. Shukla AK, Ravikumar MK, Arico AS, Candiano G, Antonucci V, Giordano N, Hamnett A (1995) J Appl Electrochem 25:528